

Original Article

Photocatalytic degradation of organic dye using green synthesized Mn_2O_3 nanoparticles

R. Rekha, G. Gurumoorthy, and P. Paulraj*

*Department of Chemistry, Faculty of Arts and Science,
Bharath Institute of Higher Education and Research, Selaiyur, Chennai, Tamilnadu, India*

Received: 30 May 2022; Revised: 15 October 2022; Accepted: 20 October 2022

Abstract

Nowadays, the usage of metal and metal oxide nanoparticles has increased in various fields. This demand leads to a mass manufacture via energy intensive techniques using numerous toxic solvents. Green technology would be an ideal method for producing metal and metal oxide nanoparticles avoiding environmental contamination, promoting low toxicity, safety for human health, environmental compatibility, and low costs. Azadirachta indica (Neem leaf) extract was used in a green approach to the production of manganese dioxide, and manganese (III) oxide nanoparticles (Mn_2O_3 NPs) were produced by a thermal decomposition method. Various instrumental analyses confirmed the cubic crystalline form, coarse sphere-like morphology with a grain size of 30 nm, and band gap energy of 4.0 eV. In these investigations, Mn_2O_3 NPs were used as a heterogeneous catalyst for the degradation of Rhodamine B (RhB) under sunlight irradiation. The study confirmed a good photocatalytic activity in terms of the rate constant of $1.4 \times 10^{-2} \text{ min}^{-1}$ and the reusability results showed that the product can be reused for up to five times without losing its efficiency.

Keywords: green synthesis, Mn_2O_3 NPs, Azadirachta indica (Neem leaf), photocatalytic degradation, rhodamine B**1. Introduction**

Metal or metal oxide nanoparticles have acquired extraordinary appeal due to their intriguing physical, chemical, magnetic, optical, and biological features. Generally, physical, chemical, and biological techniques are used to create metal-based nanoparticles. From these, biological approaches are recommended because of their ease, green aspects, straightforwardness, quickness, eco-friendliness, and economy. Here, the preparation of metal oxide nanoparticles by using a plant extract plays a vital role, reducing for the usage of numerous toxic solvents and energy intensive techniques. The plant extract contains some phytochemical compounds, which mainly act as stabilizers and reducing agents (Ponnusamy, Venkatesan, Kandasamy, & Cote, 2019).

Manganese oxide (MnO_2) is a non-stoichiometric n-type semiconductor that exists in a variety of polymorphic and

crystallographic phases due to its unique special and corner-sharing arrangements, resulting in a wide range of physical and chemical properties (Guo, Yu, Li, & Cote, 2019; Massa *et al.*, 2019; Shi *et al.*, 2018). It is chemically stable, easy to synthesize, mildly corrosive, has changeable oxidation state, and is environmentally beneficial (Le, Wang, Tran, & Cote, 2017; Li *et al.*, 2017; Wang, *et al.*, 2015). MnO_2 is used as a photocatalyst (Cao, Li, Wang, & Cote, 2015; Sundari *et al.*, 2018; Zhao *et al.*, 2017), gas sensor (Shalini *et al.*, 2019; Si, Wang, Peng, & Cote, 2015), biosensor (Han, Shao, Liang, & Cote, 2016; Zhang *et al.*, 2018), electrochemical sensor (Zhang, & Zheng, 2016), and it is prepared using various methods to various morphologies such as nanorods (Kumar, Bhaumik, Sen, & Cote, 2017), nanowires, nanospheres (Blessi *et al.*, 2021), cubes (Wang, Ding, Wang & Cote, 2016), nanourchins (Zhang *et al.*, 2018), nano-flowers, hollow cubes, nanosheets (He, Jiang, Chen, & Cote, 2018; Paulraj *et al.*, 2021; Zhang *et al.*, 2020), and more.

Mn_2O_3 has both amorphous and crystalline forms and it is an inexpensive, sustainable substance that can be found in various polymorphs. Due to the presence of crystalline structural defects in its atomic arrangements, α -

*Corresponding author

Email address: pandijothipaulraj@gmail.com

Mn₂O₃ acts as an excellent photocatalyst due to significant properties of charge transfer resistance, and it has the ability to form heterojunctions to enhance the e/h⁺ pair separation. These characteristics enhance sensitivity and adsorption capacity in the presence of UV and visible light irradiation (Jassby, Farnar, Budarz, Wiesner, & Cote, 2012; Moharreri *et al.*, 2018; Zhao *et al.*, 2017).

Mn₂O₃ nanoparticles were prepared by Najjar *et al.*, using a simple co-precipitation method with varying pH (Najjar, Awad, Abdel-Gaber, & Cote, 2019). Khalaji *et al.* used thermal breakdown methods to synthesize nanoparticles from a complex (Khalaji & Ghorbani, 2018). Sadeq and colleagues produced Mn₂O₃ in order to analyse its structural and optical properties and investigate its antibacterial activity (Sadeq, 2019). Pudukudy *et al.* synthesized α -Mn₂O₃ nanocomposites for the degradation of orange-8 dye and examined their antibacterial activity, while Abebe *et al.* prepared PVA-aided ZnO/ Mn₂O₃ nanocomposites for the degradation of orange-8 dye and analysed their antibacterial activity (Abebe, Zereffa, Murthy, & Cote, 2021; Paulraj *et al.*, 2020). For the photocatalytic use of MB and RhB, Kalaiselvi *et al.* prepared long single crystalline α -Mn₂O₃ nanorods (Kalaiselvi *et al.*, 2020).

For the synthesis of metal oxide nanoparticles, hydrazine hydrate and sodium borohydride are generally used as reducing agents, but due to toxicity they are not preferred. To avoid environmental contamination, we prefer to pursue the synthesis of metal oxide by using some plant extract. Azadirachta indica (Neem) leaf extract is used in the synthesis of MnO₂ nanoparticles. Neem tree belongs to the Meliaceae family, which is used in traditional medicine and also is one of the fast-growing plants in India. This extract is used in various healthcare products like hair oils, Neem tooth pastes, skin care products etc. Some phytochemicals like terpenoids and flavanones are present in the Neem extract and these act as reducing as well as stabilizing agents (Patil, Chaudhari, & Nemade, 2022). The organic dyes are toxic, non-biodegradable, and carcinogenic, and they are the most common contributors of water contamination. New strategies are required to convert the toxic environmentally damaging substances to safer materials. Photocatalytic degradation is one of the easiest and most cost-effective strategies for removing hazardous dyes (Devendran, Alagesan, Nallamuthu, & Cote, 2020; Marx Nirmal *et al.*, 2011; Raja *et al.*, 2020). RhB is a type of xanthene dye that is widely used in industry. We chose RhB as our model pollutant because it is comparatively stable and slow to degrade.

Heterogeneous photocatalysis is a promising approach for the degradation of hazardous pollutants into non-toxic products. The UV light only makes up 4% of the solar spectrum, but the majority of photocatalysts can only be activated under UV light irradiation due to their wide band gap. This results in a low photo-electronic transition efficiency. Therefore, the development of highly effective visible light-driven photocatalysts for the degradation of environmental contaminants is both required and desired. Their physical and chemical characteristics can be effectively enhanced when their size is reduced to the nanoscale. Due to their unique electrical, optical, photonic, and catalytic characteristics, nanostructured metal oxides have been regarded as significant materials because they are effective at absorbing electromagnetic radiation (EMR) in the visible

region. That is why many metal oxides have been suggested for the photocatalytic degradation of organic pollutants.

2. Experimental

2.1 Materials and methods

MnCl₂·4H₂O, H₂O₂ and methanol were purchased from Aldrich chemicals, and all the remaining chemicals were purchased where locally available in analytical grade. All the stock solutions for the measurements were prepared using Millipore water.

2.1.1 Preparation of Azadirachta indica leaves extract

The leaves of Azadirachta indica (neem) were collected from our University campus. Neem leaves were air dried at RT after washing and 50 grams of leaves were finely mashed with 100 ml water. This combination was cooked for 1 hour at 60 °C. After filtration of this yellow-colored solution by Whatman 40 filter paper, it was used for biosynthesis.

2.1.2 Preparation of MnO₂ and Mn₂O₃ Nanoparticles

First to prepare MnO₂ nanoparticles, 5 mL Azadirachta indica (Neem leaf) leaf extract was added with 20 mL of aqueous 0.6 M MnCl₂·4H₂O and stirred for 1 hr. Further, 6 wt % of H₂O₂ was added drop-wise and the formed dark brown suspension was placed in visible light for one day exposed to atmospheric air and its gaseous O₂. The suspension was washed several times with copious amounts of Millipore water and CH₃OH for the removal of un-reacted starting materials. Finally MnO₂ was air-dried at room temperature for 12 h. From this MnO₂, Mn₂O₃NPs were prepared via thermal decomposition by calcination at 450-500 °C. The prepared Mn₂O₃NPs were analyzed by various instrumental techniques.

2.2 Instrumentation

The Mn₂O₃NPs were analyzed by various instrumental techniques. The electronic spectra were analyzed by a UV-Visible Spectrophotometer (SHIMADZU-1800, Japan) in the range of 200–800 nm using water as a solvent. FT-IR spectra were analyzed using Perkin-Elmer, USA (Model-Y 40) within the range of 400–4000 cm⁻¹. All FT-IR spectra were corrected against the background spectrum of KBr. The X-ray diffraction pattern (XRD) of the sample was analyzed using a Philips instrument (JSO Debye Flex 2002 Seifert) in the range of 10–70° with scanning speed of 10°/min. FE-SEM (SU6600, HITACHI Ltd., Japan, low voltage (20 kV)) and HR-TEM (JEOL-3010) were used to investigate the morphology and surface aspects of the samples synthesized.

2.3 Photocatalytic degradation of dye

The organic pollutant RhB dye was chosen to examine the photocatalytic activity of Mn₂O₃NPs. For this, 100 mg of prepared Mn₂O₃NPs was dispersed in 10 mL deionized water using sonication. The 100 ml of 1.0 × 10⁻⁵ M

RhB dye solution was added separately into the catalyst dispersed suspension, and the blend was stirred at RT for a few hours to attain the adsorption and desorption equilibrium of Mn₂O₃NPs and RhB dye, because the physical adsorption on the catalyst surface plays a vital role in photodegradation. On exposure to sunlight, the photocatalytic activity of Mn₂O₃NPs was monitored at neutral pH. After 15 minutes, a 5 ml of sample was collected and centrifuged for the complete removal of catalyst and then the solution was analyzed using a UV-visible spectrophotometer.

The pseudo first order rate constants (1) were obtained from the graphs (slope). The following formulas were used to compute the % reduction of dye (2 & 3).

$$k = \frac{2.303}{t} \ln \frac{C_0}{C} \quad (1)$$

$$\text{Percentage reduction} = \frac{\text{O.D. at initial time } (C_0) - \text{O.D. at time } t(C_t)}{\text{O.D. at initial time } (C_0)} \times 100 \quad (2)$$

where C_0 = initial concentration, C_t = concentration remaining after irradiation at time t . ΔG^\ddagger = Gibb's free energy of activation for the reduction process was calculated as

$$\Delta G^\ddagger = -RT \ln k \quad (3)$$

where k = rate constant, R = universal gas constant (8.314 J mol⁻¹K⁻¹) and T = absolute temperature in Kelvin.

2.6 Recyclability test

After completing the initial photocatalytic test, Mn₂O₃NPs were removed from the prior RhB solution, washed several times in distilled water and ethanol, and then dried in a hot oven at 120 °C. It was then utilized once more for a second photocatalytic analysis with fresh RhB solution. Identical procedures to the initial measurement were followed each time. To determine the catalytic efficiency and stability of the catalyst, the same measurement was repeated five times using the same catalyst recycled.

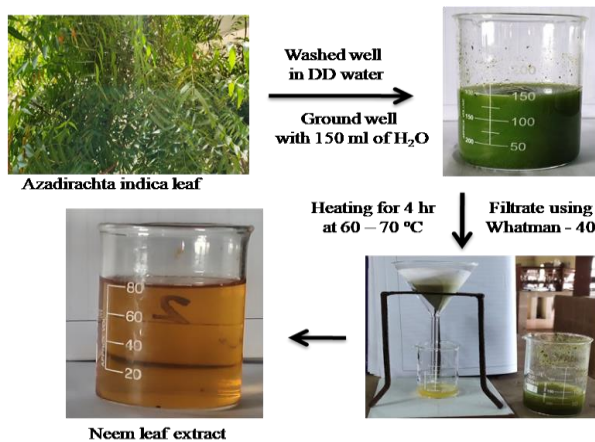


Figure 1. The process flow diagram for the preparation of Azadirachta indica leaf extract

3. Results and Discussion

3.1 UV-visible spectroscopy

Figure 2a shows the UV-visible spectra of MnO₂ (a) and Mn₂O₃NPs (b). Two peaks are seen at ~394 and ~366 nm, which clearly ensure the charge transfer transition of MnO₂ (a) and Mn₂O₃NPs (b) respectively. This lower wavelength and higher absorbance of Mn₂O₃NPs ensure its quantum confinement of the NPs and reduced size of the NPs by thermal decomposition, which leads to increased specific surface area of the NPs that is of significance when used as a photocatalyst (Najjar, Awad, Abdel-Gaber & Cote, 2019; Pugazhivadivu *et al.*, 2013). The band gap of Mn₂O₃NPs were calculated as 4.0 eV using the Tauc plot shown in Figure 2b.

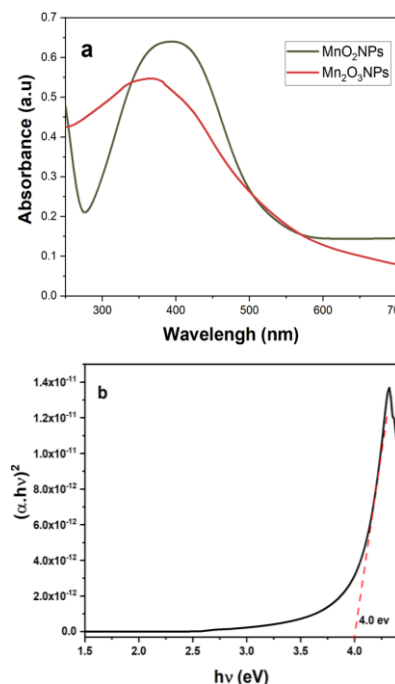


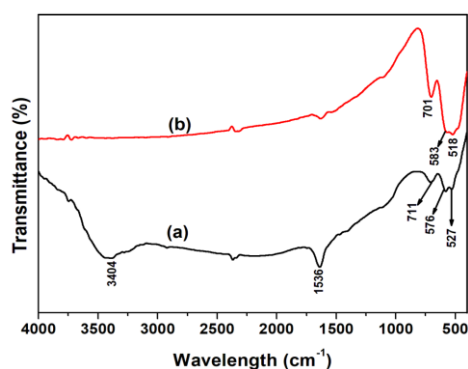
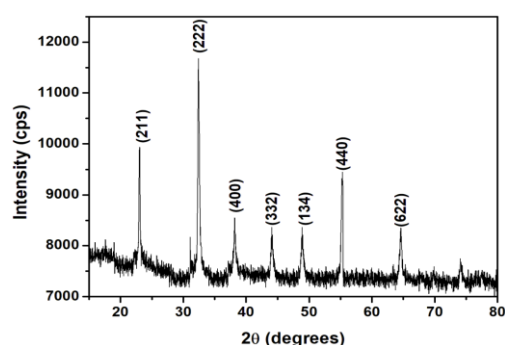
Figure 2. UV-Visible spectra (a) of MnO₂ and Mn₂O₃NPs, and (b) the Tauc plot of Mn₂O₃NPs

3.2 FT-IR spectroscopy

The comparison of FT-IR spectra of MnO₂ (a) and Mn₂O₃NPs (b) was performed in the 400-4000 cm⁻¹ range as shown in Figure 3. The strong resolved peaks at 1640 and 3417 cm⁻¹ correlate to the presence of residual O-H groups on MnO₂NPs, and two resolved peaks at 711, 509, and 463 cm⁻¹ can be attributed to the stretching vibrations of Mn-O and Mn-O-Mn bonds. Only three resolved peaks at 701, 583, and 518 cm⁻¹ were assigned to the stretching vibrations of Mn-O and Mn-O-Mn bonds in Mn₂O₃NPs in the spectrum (b). Thermal heating fully eliminated the O-H groups, as evidenced by a reduction in their corresponding reactions (Kumar, Bhaumik, Sen, & Cote, 2017; Kumar *et al.*, 2020).

3.3 X-ray diffraction

The prepared Mn₂O₃NPs was confirmed by XRD as shown in Figure 4. The diffraction peaks at 2θ of 32.5°, 38.1°, and 38.1° were assigned to the (110), (111), and (111) planes of Mn₂O₃, respectively.

Figure 3. FT-IR spectra of MnO₂ (a), and Mn₂O₃NPs (b)Figure 4. XRD spectrum of Mn₂O₃NPs

44.2°, 48.9°, 55.3° and 64.5° correspond to (211), (222), (400), (332), (134), (440) and (622) planes of cubic Mn₂O₃NPs. These patterns indicate that the corresponding metal oxide had been formed, without any evidence of impurities, and had a good match with JCPDS No. 02-0896 (Moon, Salunke, Saha & Cote, 2018). These results ensure that the synthesis of Mn₂O₃NPs by thermal decomposition and the Mn₂O₃NPs nanoparticles were purely crystalline in nature, and also the crystal parameters were determined by Debye–Scherrer formula (Equation 1).

$$d = \frac{0.90 \lambda}{\beta \cdot \cos \theta} \quad (1)$$

Here, $\lambda = 0.15406$ nm, θ = diffraction angle, and β = Full width half maximum (FWHM) value. For all peaks of Mn₂O₃NPs these were calculated using Origin version 8.0, and the crystalline characteristics and sizes are presented in Table 1. The NPs have been measured to be ~30.35 nm in size.

Table 1. Mn₂O₃NPs crystallite size and other characteristics

S.No.	(h k l)	Peak position 2θ (°)	FWHM (β)	Crystallite size (nm)
1.	(211)	23.03731	0.240146	33.76108
2.	(222)	32.44529	0.26851	30.81342
3.	(400)	38.19123	0.37694	22.303
4.	(332)	44.12205	0.326377	26.26375
5.	(134)	48.93068	0.326179	26.75815
6.	(440)	55.27084	0.215468	41.61786
7.	(622)	64.60429	0.303295	30.98911

3.4 FE-SEM analysis

FE-SEM with EDAX analysis were used to examine morphology and elemental composition of Mn₂O₃NPs as shown in Figure 5. The different magnification images gave an understanding of the details of Mn₂O₃NPs, with coarse sphere like morphology that was confirmed in HR-TEM images. The EDAX spectrum shows only manganese and oxygen as predominantly present in the sample ensuring purity of the Mn₂O₃NPs. The corresponding percentile table provides details about the proportions of elements present (Souri, Hoseinpour, Shakeri, & Cote, 2018).

3.5 HR-TEM images of Mn₂O₃NPs nanoparticles

Figure 6 shows the HR-TEM images of Mn₂O₃NPs with different magnifications, and these images ensure the cubic morphology of the analyzed sample. In addition, the dark cubic morphology indicates the presence of manganese nanoparticles with average size of 30 nm (Najjar, Awad, Abdel-Gaber & Cote, 2019).

3.6 Photocatalytic degradation of RhB

Mn₂O₃NPs were used as a photocatalyst for the degradation of RhB. Due to the inherent stability of the Mn₂O₃NPs, the RhB was degraded effectively, as confirmed by the observed hypsochromic blue shift (554 nm to 496 nm) after 210 minutes of sunlight irradiation. Figure 7b depicts the first-order reaction kinetics, which were confirmed by the linear regression fit $y = 0.014 + 0.016x$ along with a correlation coefficient of 0.9548. The apparent rate constant was obtained as $1.4 \times 10^{-2} \text{ min}^{-1}$. The rate of RhB degradation at different catalyst dosages is shown in Figure 7c. The degradation efficiency increased with catalyst dosage from 50 mg to 100 mg. It led to the removal efficiency being increased from 81% to 97%, which was achieved by increasing the production of more ·OH ions by active sites. Furthermore, on increasing the dosage to 150 mg, the rate of degradation was not improved but rather significantly decreased to 95% due to the agglomeration and scavenging of the ·OH ions, which also hindered the dispersion on the surface of the solid catalyst.

Significant changes are observed when different concentrations of RhB are tested at a constant volume of catalyst, as shown in Figure 7d. The maximum amount of RhB (97 %) was removed in 100 minutes when using 0.5×10^{-5} M/L, and when using 1.0×10^{-5} M/L concentration, 97% of RhB was removed after only 210 minutes. Furthermore, on increasing the concentration of RhB to 1.5×10^{-5} M/L, only 82.1% of the dye was removed in the prescribed time. From

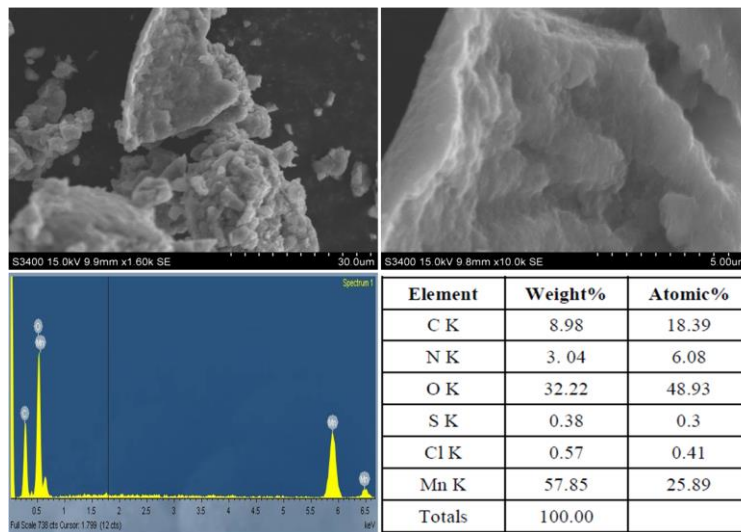


Figure 5. FE-SEM images of Mn₂O₃NPs along with EDAX and its percentile table

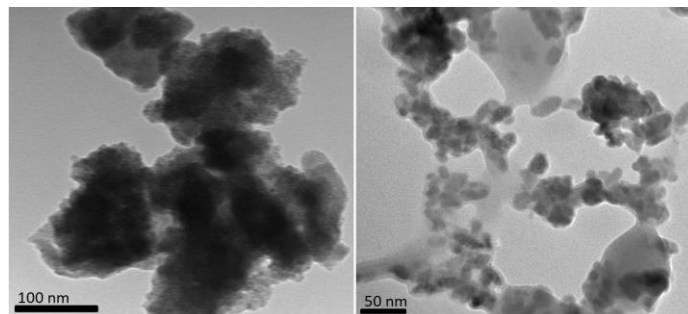


Figure 6. HR-TEM images of Mn₂O₃NPs

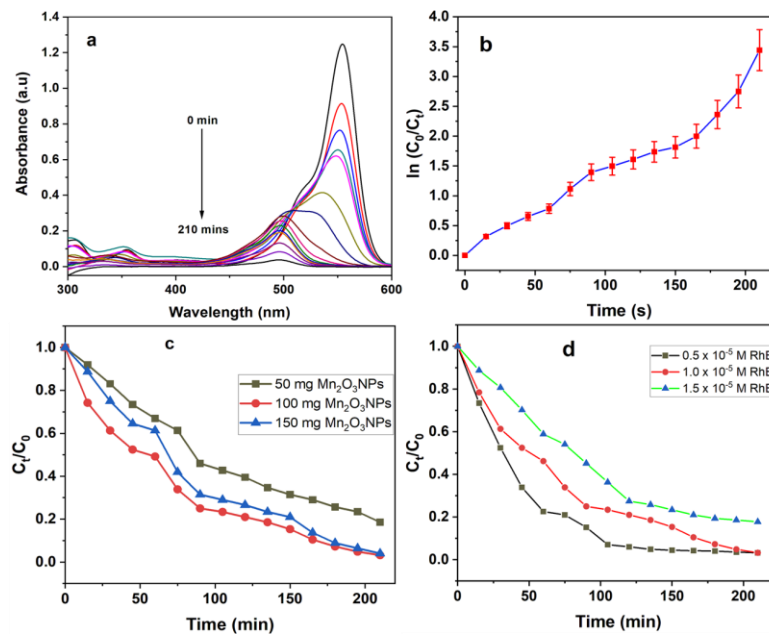


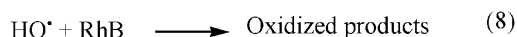
Figure 7. Time profiles of photocatalytic degradation of RhB (a) using Mn₂O₃ nanocatalyst, and (b) the corresponding calibration plot with error bars representing the standard deviations of duplicate runs. (c) The effects of three amounts of catalyst in 1.0 x 10⁻⁵ M RhB, and (d) the effects of 100 mg catalyst on three concentrations of RhB

these results, we chose 100 mg as the dosage that was most efficient for the degradation of 1.0×10^{-5} M/L of RhB.

3.7 Degradation mechanism

Three steps are involved to improve the catalyst efficiency, which are (1) generating more electron-hole pairs by harvesting a large spectrum of sunlight, (2) improving photon to electron conversion efficiency, and (3) increasing the lifetime of photo-generated electron-hole pairs. Figure 8 depicts the basic mechanism for the photocatalytic degradation of organic dye using visible light irradiation. Here, Mn_2O_3 NPs are used as visible light drivable catalysts for the removal of RhB. During photocatalysis, the valence band electron (e^-) is photoexcited into the conduction band, thereby generating a positive electron hole (h^+) in the valence band and avoiding charge separation. The excess energy is dissipated by electron-hole charge carriers ($h^+_{VB} + e^-_{CB}$) via a non-radiative mechanism. These electron-hole pairs move to the Mn_2O_3 NPs surface to take part in the oxidation-reduction reaction. Since the conduction band of Mn_2O_3 NPs is nearly isoenergetic with the reduction potential of oxygen, some of the photogenerated electrons would recombine with holes in the VB, while others would be transferred to the surface of the catalyst.

Here, molecular oxygen can scavenge electrons from the Mn_2O_3 NPs conduction band and convert to superoxide anion radical ($O_2^{\cdot-}$) (Equation 4). Then this radical forms hydrogen peroxide (H_2O_2) followed by hydroxyl radical ($\cdot OH$) when reacting with protons (Equation 5), and the hole (h^+) in the valence band generates $\cdot OH$ ions from H_2O (Equation 6). The RhB was oxidized as a result of the continuous attack of $O_2^{\cdot-}$ and $\cdot OH$ radicals (Equation 7). Furthermore, the RhB was adsorbed on Mn_2O_3 NPs and it was stimulated to an excited state under visible light irradiation. Then, through photosensitization, photoexcited dye electrons may be injected into the conduction band of the Mn_2O_3 NPs. Moreover, the photo-excited holes in the valence band degraded the RhB (Equation 8). The following equations depict these possible mechanisms and effects of reactions.



3.8 Reusability

The recovery and reusability of the Mn_2O_3 NPs is important in this experimental investigation. Mn_2O_3 NPs serve as a heterogeneous catalyst that is easily separable and can be reused again and again. In its practical utilization, the retention of efficiency is an important criterion. From Figure 9, the Mn_2O_3 NPs retained their original catalytic activity even

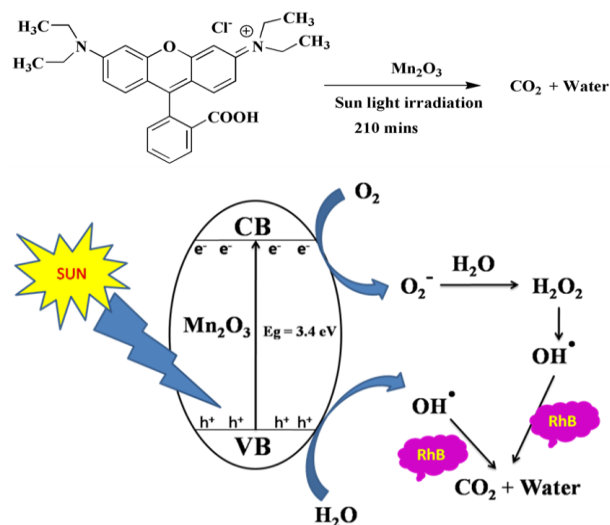


Figure 8. Photocatalytic dye degradation mechanism of RhB on using Mn_2O_3 NPs

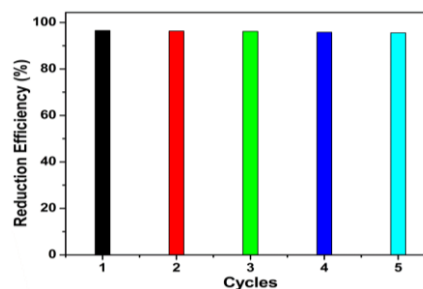


Figure 9. Reusability of Mn_2O_3 NPs

after 5 cycles. Therefore, Mn_2O_3 NPs are highly stable, highly efficient, and well recyclable, which has made them very promising for environmental remediation.

4. Conclusions

In summary, *Azadirachta indica* extract was used to synthesize Mn_2O_3 NPs by green approach, and the Mn_2O_3 NPs were successively synthesized by thermal decomposition. The morphology, shapes, sizes, and composition of Mn_2O_3 NPs were confirmed by the instrumental techniques FE-SEM, HR-TEM, XRD, and EDX. In this present investigation, Mn_2O_3 NPs were used as a heterogeneous catalyst for the removal of an organic contaminant, specifically RhB. The band gap of Mn_2O_3 NPs was obtained as 4.0 eV from the Tauc plot. The inherent stability of Mn_2O_3 NPs was tested using three different dosages, and the dye degradation rate was analyzed using three different concentrations of RhB. Among these cases, 0.1 g of Mn_2O_3 NPs removed 97% of 1.0×10^{-5} M/L of RhB in 210 minutes at neutral pH, and the rate constant was found to be $1.64 \times 10^{-2} \text{ min}^{-1}$. Mn_2O_3 NPs retained their original catalytic activity even after 5 cycles. Therefore, Mn_2O_3 NPs are highly stable, highly efficient, and well recyclable, which has made them prominent for environmental remediation.

Acknowledgements

The authors thank to Bharath University and University of Madras for providing lab and instrumental facilities to complete this work.

References

- Abebe, B., Zereffa, E. A., & Murthy, H. C. A. (2021). Synthesis of poly(vinyl alcohol)-aided ZnO/MnO nanocomposites for acid orange-8 dye degradation: Mechanism and antibacterial activity. *ACS Omega*, 6, 954-964.
- Asif, S. A. B., Sher Bahadar Khan, & Abdullah M. Asiri, A. M. (2015). Visible light functioning photocatalyst based on Al₂O₃ doped Mn₃O₄ nanomaterial for the degradation of organic toxin. *Nanoscale Research Letters*, 10, 355(1-10)
- Blessi, S., Manikandan, A., Anand, S., Sonia, M. M. L., Maria Vinosel, V., Paulraj, P., Slimani, Y., . . . Baykal, A. (2021). Effect of zinc substitution on the physical and electrochemical properties of mesoporous SnO₂ nanoparticles. *Materials Chemistry and Physics*, 273, 125122.
- Cao, J., Li, X., Wang, Y., Walsh, F. C., Ouyang, J. H., Jia, D., & Zhou, Y. (2015). Materials and fabrication of electrode scaffolds for deposition of MnO₂ and their true performance in supercapacitors. *Journal of Power Sources*, 293, 657-674.
- Devendran, P., Alagesan, T., Nallamuthu, N., Asath Bahadur, S., & Pandian, K. (2020). Single-precursor synthesis of sub-10 nm CdS nanoparticles embedded on graphene sheets nanocatalyst for active photo degradation under visible light. *Applied Surface Science*, 534, 147614.
- Guo, W., Yu, C., Li, S., Wang, Z., Yu, J., Huang, H., & Qiu, J. (2019). Strategies and insights towards the intrinsic capacitive properties of MnO₂ for supercapacitors: Challenges and perspectives. *Nano Energy*, 57, 459-472.
- Han, L., Shao, C., Liang, B., & Liu, A. (2016). Genetically engineered phage-templated MnO₂ nanowires: synthesis and their application in electrochemical glucose biosensor operated at neutral pH condition. *ACS Applied Materials and Interfaces*, 8, 13768-13776.
- He, Y., Bin Jiang, D., Chen, J., Jiang, D. Y., & Zhang, Y. X. (2018). Synthesis of MnO₂ nanosheets on montmorillonite for oxidative degradation and adsorption of methylene blue. *Journal of Colloid and Interface Science*, 510, 207-220.
- Jassby, D., Farner Budarz, J., & Wiesner, M. (2012). Impact of aggregate size and structure on the photocatalytic properties of TiO₂ and ZnO nanoparticles. *Environmental Science and Technology*, 46, 6934-6941.
- Kalaiselvi, C., Ramesh Aravind, M., Revathi, B., Nirmala Grace, A., Sudhagar, P., & Krishna Chandar, N. R. (2020). Long single crystalline α -Mn₂O₃ nanorods: Facile synthesis and photocatalytic application. *Materials Research Express*, 7, 074001.
- Khalaji, A. D., & Ghorbani, M. (2018). Mn₂O₃ nanoparticles synthesized from thermal decomposition of manganese(II) Schiff base complexes. *Acta Physica Polonica A*, 133, 7-9.
- Kumar, N., Bhaumik, S., Sen, A., Shukla, A. P., & Pathak, S. D. (2017). One-pot synthesis and first-principles elasticity analysis of polymorphic MnO₂ nanorods for tribological assessment as friction modifiers. *RSC Advances*, 7, 34138-34148.
- Kumar, Y., Chopra, S., Gupta, A., Kumar, Y., Uke, S. J., & Mardikar, S. P. (2020). Low temperature synthesis of MnO₂ nanostructures for supercapacitor application. *Materials Science for Energy Technologies*, 3, 566-574
- Le, Q. J., Wang, T., Tran, D. N. H., Dong, F., Zhang, Y. X., & Losic, D. (2017). Morphology-controlled MnO₂ modified silicon diatoms for high-performance asymmetric supercapacitors. *Journal of Materials Chemistry A: Materials for Energy and Sustainability*, 5, 10856 - 10865.
- Li, X., Ding, R., Shi, W., Xu, Q., Wang, L., Jiang, H., . . . Liu, E. (2017). Hierarchical mesoporous Ni-P/MnO₂ composite for high performance supercapacitors. *Materials Letters*, 187, 144-147.
- Marx Nirmal, R., Paulraj, P., Pandian, K., & Sivakumar, K. (2011). Preparation, characterization and photocatalytic properties of CdS and Cd_{1-x}Zn_xS nanostructures. *AIP Conference Proceedings*, 1391, 597-599.
- Moharreri, E., Hines, W. A., Biswas, S., Perry, D. M., He, J., Murray-Simmons, D., & Suib, S. L. (2018). Comprehensive magnetic study of nanostructured mesoporous manganese oxide materials and implications for catalytic behavior. *Chemistry of Materials*, 30, 1164-1177.
- Moon, S. A., Salunke, B. K., Saha, P., Deshmukh, A. R., & Kim, B. (2018). Comparison of dye degradation potential of biosynthesized copper oxide, manganese dioxide, and silver nanoparticles using *Kalopanax pictus* plant extract. *Korean Journal of Chemical Engineering*, 35, 702-708.
- Najjar, R., Awad, R., & Abdel-Gaber, A. M. (2019). Physical properties of Mn₂O₃ nanoparticles synthesized by co-precipitation method at different pH values. *Journal of Superconductivity and Novel Magnetism*, 32, 885-892.
- Paulraj, P., Ahmad Umar, Rajendran, K., Manikandan, A., Sathamraja, A., Kumar, R., Manikandan, E., . . . Alsaiari, M. A. (2021). Methylene blue intercalated layered MnO₂ nanosheets for high-sensitive non-enzymatic ascorbic acid sensor. *Journal of Materials Science: Materials in Electronics*, 3, 1-13.
- Paulraj, P., Rajendran, K., Sathamraja, A., Pandian, K. (2021) Solid phase mechanochemical synthesis of Poly(o-anisidine) protected Silver nanoparticles for electrochemical dopamine sensor. *Materials Today Communications*, 26, 102191.
- Ponnusamy, R., Venkatesan, R., Kandasamy, M., Chakraborty, B., & Rout, C. (2019) MnO₂ polymorph selection for non-enzymatic glucose detection: An integrated experimental and density

- functional theory investigation. *Applied Surface Science*, 487, 1033-1042.
- Rafique, Massa, A., Fontana, M., Bianco, S., Chiodoni, A., Pirri, C. F., . . . Lamberti, A. (2017). Highly uniform anodically deposited film of MnO₂ nanoflakes on carbon fibers for flexible and wearable fiber-shaped supercapacitors. *ACS Applied Materials and Interfaces*, 9, 28386–28393.
- Raja, A., Rajasekaran, P., Selvakumar, K., Arivanadhan, M., Asath Bahadur, S., & Swaminathan, M. (2020). Rational fabrication of Needle with spherical shape ternary reduced Graphene Oxide-HoVO₄-TiO₂ photocatalyst for degradation of ibuprofen under visible light. *Applied Surface Science*, 513, 145803.
- Sadeq, Z. S. (2019). Structural and optical study of Mn₂O₃ nanoparticles and its antibacterial activity. *SYLWAN*, 161, 76-84.
- Shalini, A., Paulraj, P., Pandian, K., Anbazhagan, G., & Jaisankar, V. (2019). Synthesis and characterization of graphene oxide coated au nano particles and the study of its application on electro catalytic activity of nitric oxide. *Advanced Materials Proceedings*, 4(4), 158-161.
- Shi, X., Li, Y., Chen, R., Ni, H., Zhan, W., Zhang, B., . . . Dong, S. (2018). Defective carbon nanotube forest grown on stainless steel encapsulated in MnO₂ nanosheets for supercapacitors. *Electrochimica Acta*, 278, 61-71.
- Patil, S. P., Chaudhari, R. Y., & Nemade, M. S. (2022). Azadirachta indica leaves mediated green synthesis of metal oxide nanoparticles: A review. *Talanta Open*, 5, 100083.
- Si, W., Wang, Y., Peng, Y., Li, X., Li, K., & Li, J. (2015). A high-efficiency c-MnO₂-like catalyst in toluene combustion. *Chemical Communications*, 51, 14977-14980.
- Souri, M., Hoseinpour, V., Shakeri, A., & Ghaemi, N. (2018). Optimisation of green synthesis of MnO nanoparticles via utilising response surface methodology. *IET Nanobiotechnology*, 12, 822–827
- Sundari, R., Alva, S., Sebayang, D., Wahyudi, H., Jonit, S., & Kamaruddin, A. (2018). Characterization of fabricated MnO₂-amberlite photocatalyst by FTIR, XRD and SEM for alizarin removal. *IOP Conference Series: Materials Science and Engineering*, 343, 012003
- Wang, J., Kang, F., & Wei, B. (2015). Engineering of MnO₂-based nanocomposites for high-performance supercapacitors. *Progress in Materials Science*, 74, 51-124.
- Wang, Y., Ding, P., & Wang, C. (2016). Fabrication and lithium storage properties of MnO₂ hierarchical hollow cubes. *Journal of Alloys and Compounds*, 654, 273-279.
- Zhang, L., Chen, Q., Han, X., & Zhang, Q. (2018). MnO₂ Nanoparticles and carbon nanofibers nanocomposites with high sensing performance toward glucose. *Journal of Cluster Science*, 29, 1089-1098.
- Zhang, S., & Zheng, J. (2016). Synthesis of single-crystal a-MnO₂ nanotubes-loaded Ag@C core-shell matrix and their application for electrochemical sensing of nonenzymatic hydrogen peroxide. *Talanta*, 159, 231-237.
- Zhang, T., Kong, L., Dai, Y., Yue, X., Rong, J., Qiu, F., & Pan, J. (2017). Enhanced oils and organic solvents absorption by polyurethane foams composites modified with MnO₂ nanowires. *Chemical Engineering Journal*, 309, 7-14.
- Zhang, Y., Wang, F., Ou, P., Zhu, H., Lai, Y., Zhao, Y., . . . Wang, T. (2018). High efficiency and rapid degradation of bisphenol A by the synergy between adsorption and oxidization on the MnO₂@nano hollow carbon sphere. *Journal of Hazardous Materials*, 360, 223-232.
- Zhang, Y., Yang, Z., Li M., Yang, L., Liu, J., Ha, Y., & Wu, R. (2020). Heterostructured CoFe@C@MnO₂ nanocubes for efficient microwave absorption. *Chemical Engineering Journal*, 382, 123039.
- Zhao J., Nan, J., Zhao, Z., Li, N., Liu, J., & Cui, F. (2017). Energy-efficient fabrication of a novel multivalence Mn₃O₄-MnO₂ heterojunction for dye degradation under visible light irradiation. *Applied Catalysis B: Environmental*, 202, 509-517.
- Zhao, J., Nan, J., Zhao, Z., & Li, N. (2017). Facile fabrication of novel Mn₂O₃ Nanocubes with superior light-harvesting for ciprofloxacin degradation. *Catalysis Communications*, 102, 5–8.